Testing the reliability of detrital cave sediments as recorders of paleomagnetic secular variations, Seso Cave System (Central Pyrenees, Spain)

Belén Oliva-Urcia[1,2,3], Miguel Bartolomé[1], Ana Moreno[1], Graciela Gil-Romera[1], Carlos Sancho[3], Arsenio Muñoz[3], Mª Cinta Osácar[3]

1.Instituto Pirenaico de Ecología-CSIC. Avda. Montañana 1005. 50059 Zaragoza. Spain.
Phone:(+34)976369393(EXT880056)
Fax:(+34) 976 716 019. boliva@ipe.csic.es
2.Dpto. Geología y Geoquímica. Universidad Autónoma de Madrid. Ciudad Universitaria de Cantoblanco · 28049 Madrid. belen.oliva@uam.es
3.Dpto. Ciencias de la Tierra, Universidad de Zaragoza, Pedro Cerbuna 12, 50009 Zaragoza, Spain

Abstract

A paleomagnetic study has been carried out on a waterlaid detrital sedimentary sequence of ~ 240 cm thick within the Seso Cave System (West-Central Pyrenees). In these sediments, seven charcoal samples were dated using ^{14}C AMS ranging from 2080 to 650 cal yr BP (130 BC-1300 AD). Two levels of human occupation of the cave have been recognized by ceramics associated to the Iberian Period and to the Roman Period, respectively. The detrital sedimentary sequence is made of autochthonous (piping detached material from the Eocene marls host rock inside of the cavity) and allochthonous (stream transported sediments from the outside) sediments. The autochthonous material (first 100 cm), made of fine grain laminated sediments (lutites and marls) corresponds to pond facies; the allochthonous material (190-240 cm) is made of lutites and sands and corresponds to stream facies, and both facies are mixed from 100 to 190 cm. The increase in sedimentation rate towards the end of the sequence (stream facies) points to an intensification of the alluvial activity as a possible consequence of a more arid climate during the Medieval Climate Anomaly. For the paleomagnetic study, 44 discrete cylindrical samples were taken along the detrital sequence. The values of the natural remanent magnetization and magnetic susceptibility are significantly lower in the pond sediments than in the stream sediments. The declination and inclination of the paleomagnetic characteristic component (sister

samples analyzed by both alternating field and temperature demagnetizing procedure) of each depth point is compared to the Spanish archeomagnetic catalogue and available geomagnetic models (ARCH3k.1, CALS3k.4, CALS10k.1band SCHA.DIF.3k) in order to determine the accuracy of these sediments recording the Earth magnetic field. Results suggest that these sediments poorly record the Earth magnetic field, however, paleomagnetic inclination shows similar results between both demagnetizing methods and the inclination is well recorded especially in the younger stream facies. The lack of archeological remains with absolute dates from 925 to 1545 cal yr BP. in the Iberian paleomagnetic secular variation reference curve has prevented, up to now, the study of that time period. Therefore, the inclination data from the Seso Cave deposit is the first record of the Iberian paleomagnetic secular variation during most part of Medieval times, and they are closer to the inclination values of one geomagnetic model (CALS10k.1b).

Key words: paleomagnetic secular variation, detrital cave sediments, Seso Cave System, Holocene, NE Spain

1. Introduction

The classical theory of the acquisition of the characteristic magnetization in sediments (detrital remanent magnetization –DRM–) was already proposed by Nagata (1961). The Earth's magnetic field imposes a torque on the magnetic particles, which tends to align them with the field therefore the magnetic grains align during deposition. However, for the last three decades the concept is being under consideration, in the light of, for example, the influence of postdepositional effects in the orientation of the magnetic moment of the particles due to e.g. physical compaction. As a result of postdepositional compaction, shallowing inclination errors have been documented in red beds (Tan and Kodama, 2002 and references therein). Therefore, the postdepositional effects on the magnetic particles can affect, and also delay, the final acquisition of the DRM, then the remanent acquisition is called postdepositional remanent magnetization (pDRM) and it can be influenced by many factors, among them: grain size, rate of deposition, bioturbation, diagenetic processes, biochemical origin of new minerals (Butler, 1992; Abrajevitch and Kodama, 2009; Bilardello et al., 2013 and references therein).

In addition to the postdepositional modifications, the depositional effects such as the physical-chemical properties of the fluids and particles can also affect the alignment of the magnetic particles before they reach the sediment – water interface. Flocculation of particles during deposition affects the final alignment of the magnetic particles with the magnetic field. The influence of some depositional processes on flocculation have been studied in models and redeposition experiments considering salinity, composition of sediments, pH characteristics of the depositional environment or shape of particles (Katari et al., 2000; Mitra and Tauxe, 2009; Bilardello et al., 2013). These experiments suggest that the alignment of the magnetic particles with the magnetic field seems to be better for carbonate rich sediments, with lower clay content, therefore the former sediments are more suitable for relative paleointensity record (Spassov and Valet, 2012 and references therein).

The paleomagnetic record of continental sediments can be used as a chronological tool using the record of the inversions of the Earth magnetic field. This inversions of the Earth magnetic field are marked for changes in the values of the paleomagnetic inclination, i.e. positive inclination and northern declination in normal polarity periods, to negative inclination and southern declination in reversal polarity periods, in the northern hemisphere. The sequence of inversions at local scale is then compared with the geomagnetic polarity time scale (GPTS) (Gradstein et al., 2004) for dating purposes. This is possible to apply in long sedimentary sequences and older than 780,000 yr, when the last inversion from reverse to normal polarity chron occurs. In short sedimentary sequence (i.e., karstic sediments) the anchoring of one of the local polarity variations is necessary. The anchoring can be done with an independent dating technique i.e., relative dating linked to the speleogenesis of the cave, ^{14}C, and optical stimulated luminescence among others. Otherwise magnetostratigraphic dating can be problematic (Bosák et al., 2003). In younger sediments (< 780,000 yr) polarity is always normal (except for at least 5 short excursions of the Earth magnetic field, Channel, 2006) therefore changes in polarity are no longer valid for dating purposes. Then, the secular variations of the Earth magnetic field are used as a chronological framework. Secular variations are short-term variations of the Earth magnetic field that can be recorded at one location by changes in declination, inclination and intensity. However, the construction of secular variations curves is usually limited to the paleomagnetic data from archeomagnetic structures (kilns), which have been dated by other techniques. In

particular, the catalogue of secular variations in Iberia spans less than ~2,000 yr BP (Gómez-Paccard et al., 2006). There are examples where secular variation data have been used to date archeomagnetic artifacts when other dating technique is not available (Gómez-Paccard and Beamud, 2008). In addition to the actual data, there are also numerical models that reproduce the secular variations for the past (back to few million of years) based on archeomagnetic and paleomagnetic data of sediments (Korte and Constable, 2011; Korte et al., 2011; Pavón-Carrasco et al., 2009 among others).

Quaternary waterlaid detrital sediments in karstic caves are very particular since their deposition is spatially restricted and highly controlled by several different sedimentation processes and speleogenesis. However, caves often house clastic sedimentary records containing valuable palaeoenvironmental as well as chronological indicators. Sediments can be reworked from the cave material itself (internal or autochthonous origin), i.e. insoluble residue from bedrock, remobilization and deposition of sediments within the cave conduit; or they may come from the exterior (external or allochthonous origin) i.e: injection of allogenic soils by sinking streams, soils infiltration through joints and fractures, storm inwash of soils, piping failures or sinkhole collapses (Bosch and White, 2007; Ford and Williams, 2007). Stream deposits including sands, silts and clays are widespread clastic deposits in caves. Stream and pond deposits are common waterlaid clastic sediments in caves (Jennings, 1985) in interior sequences in a similar way to alluvial systems in surface (Bosch and White 2007). Changes in the sedimentary facies indicate changes in the processes of deposition of particles with time. Although these waterlaid detrital sediments have suitable characteristics for paleomagnetic analysis, very scarce information on this indicator is available at the moment. Only some attempts to study paleomagnetism in Pleistocene-Holocene detrital sequences are reported (Faust et al., 2004; Zielhofer et al., 2008; Gómez-Paccard et al., 2013) and some correspond to cave sediments (Creer and Kopper, 1974; Creer and Kopper, 1976; Noel and Pierre, 1984; Noel and Shaw, 1984; Noel, 1986; Turner and Lyons; 1986). More recently, the recording of inversions of the paleomagnetic field is analyzed in old cave sediments for dating purposes (Sasowsky et al., 1995; Bosák et al., 2003; Stock et al., 2005; Musgrave and Webb, 2007; Chazan et al., 2008; Herries and Saw, 2011). These studies indeed confirm that the sediments within caves can record the polarity of the Earth magnetic field.

Our study is focused on the paleomagnetic signature of a Holocene waterlaid detrital

sequence housed in the Seso Cave System (West-Central Pyrenees). The purpose of this study is to compare the results of the calculated characteristic component to: i) the known secular variation data of Iberia for the last 2,000 yr (Gómez-Paccard et al., 2006), ii) three global geomagnetic field models, ARCH3k.1, CALS3k.4 and CALS10k.1b (Donadini et al., 2006; Korhonen et al., 2008, Korte and Constable, 2011; Korte et al., 2011) iii) Pavón-Carrasco et al. (2009) regional geomagnetic model for the last 3,000 yr (SCHA.DIF.3k) in order to qualitatively, measure the accuracy of the recording of the Earth magnetic field in two distinct cave deposits (pond and stream sediments) analyzing for that purpose discrete samples and using the two standard demagnetizing methods (alternating field and thermal).

2. The Seso Cave System

The Seso Cave System (SCS) is located near Boltaña (Huesca), in the eastern limb of the Boltaña anticline (Mas and Fuertes, 2007; Bartolomé et al., 2011), which represents the structural boundary between the South Pyrenean Central Unit to the east and the Jaca-Pamplona basin to the west, in the southern Pyrenees (Séguret, 1972; Soto and Casas, 2001) (Fig. 1, 1a). The Eocene marls and limestones (Boltaña Formation) host the SCS. It is basically a pseudokarstic cave system developed by piping processes affecting Eocene marls (Bartolomé et al., 2011, 2013). Two caves and a seasonal spring in the lowest part form this pseudo-karst system (Fig. 1b). The main speleogenetic mechanism is the intrastratal subsurface piping processes that affect the highly dispersive marls (Bartolomé et al., 2013). As a consequence, cave speleogenesis involves the mechanical washout of large amounts of fine sediments moving along the galleries. On the other hand, SCS houses interesting stalagmites recording the climate variability during the end of Upper Pleistocene and Holocene times (Bartolomé et al., 2011).

This study is carried out in the lower cave of the SCS (763 m.a.s.l). The cave presents 147 m of longitudinal development, 21 m of vertical gradient (between +3 and -18 m, taking as 0 m the level of the entrance) and three entrances (two in the upper part and one in the lower part). The studied detrital profile is located in the lowest part of the cave (Fig. 1c, 1d).

The present day climate is classified as under the influence of the transition of Mediterranean-Atlantic climate (López et al., 2007). Precipitations are 1021 mm / yr and they occur during spring and autumn-winter due to Atlantic fronts, disturbances and equinoctial maxima from the Mediterranean environment. Averaged temperatures are 2.8ºC in January and 24.3ºC in July, with the annual mean of 12ºC (López et al., 2007). Respect to vegetation, forest and shrubs cover the slopes. Pines (*Pynus sylvestris*) and oaks (*Quercus ilex*) dominate the forested areas, whereas boxes (*Buxus sempervirens*), gorses (*Ulux parviflorus*), rosemary (*Rosmarius officinalis),* A*phyllanthes monspeliensis* and a variety of *Gramineae* species are abundant in the shrubs areas.

The generalized alteration of the marls covering the cave-surrounding slopes yields to a cambic calcisol soil as in the World Reference Base for Soil Resources (IUSS, 2007). The soil develops over a tilted slope ~ 20º - 25º and it presents irregular thickness, which can reach up to 2 m near the cave entrance. The surficial horizon (A) has dark colors and granular texture. Underneath (B horizon), there is a generalized change in color, from the grey color of the marl to brown and oranges tones and an enrichment in carbonates in the shape of white nodules (< 2 mm diameter). The B horizon grades into a C horizon. The soil is relatively well preserved, although locally has been totally eroded. These moderately developed soils are frequent in subhumid mountainous areas at regional scale.

3. Methods

Only one stratigraphic profile was described and interpreted because of the reduced size of the detrital sedimentary deposits in the Seso Cave System. Several proposals of classification of clastic sediments in caves were made by Jennings (1985), White (1988), Bosch and White (2007) and Ford and Williams (2007). In this study we use the nomenclature by Jennings (1985). Thus clastic cave sediments include i) breakdown, weathering and mass movement deposits and ii) stream and pond deposits.

3.1. Age model reconstruction

Seven charcoal samples were analyzed by AMS in the Laboratory of DirectAMS Radiocarbon Dating System of Seattle (USA). The obtained absolute ages (Table 1) were calibrated and depth-age modeled with the package for R (R Development Core

193 Team, 2011) BACON (Blaauw and Christen, 2011). Calibration curve was INTCAL13
194 (Reimer et al., 2013) implemented in BACON and resulting ages range from 2080 to
195 650 cal yr BP (Table 1). This software performs a methodology based on controlling
196 core accumulation rates using a gamma autoregressive semi-parametric model with an
197 arbitrary number of subdivisions along the sediment, following the Bayesian approach
198 defined by Blaauw and Christen (2011). This method implies adding some prior
199 knowledge on the evolution and shape of accumulation rates, which serves as a
200 smoothness factor for the age series, followed by a self-adjusting MCMC (Monte-Carlo
201 Markov Chain) in order to build up a robust-to-outliers age model. The latter involves
202 an adaptive algorithm that learns about the modeled process to automatically tune the
203 MCMC simulation (Blaauw and Christen, 2011). Thus, the priors of the model include
204 the fact that different sections of a sequence could have been deposited with distinct
205 accumulation rates. This means that low variation in the accumulation rates throughout
206 the deposit implies a high "memory", or internal dependence amongst sections of the
207 sequence, which is a value that can be specified, as the autoregressive gamma model
208 enables defining prior settings that can be applied to the different sections of the core.
209 Therefore, this procedure demands inputting the mean accumulation rate expected and
210 the prior for the variability of accumulation rate, or "memory level". Additionally, it is
211 necessary to define the number of sections of the core in which the MCMC process will
212 be repeated.

213 For the Seso detrital record the priors were set in as follows: i) There is not previous
214 knowledge on the potential sedimentation rate of the sequence and its variability.
215 However, presuming no drastic centennial environmental changes, altering massively
216 the variability of the accumulation rate between 2000 and 600 cal yrs BP, we chose a
217 relatively high memory level (memory strength = 100 and memory mean = 0.7). ii) The
218 number of sections of the core was set at 24 as every section modeled was ca. 10 cm
219 (steps Dc = 10 cm). This value indicates the length of the sections where the MCMC
220 process will experience a renewal.

221 In addition, pottery remnants from the two described levels (-4 cm and 120-140 cm) that
222 are related to human settlements inside the cave were cleaned, identified and classified.
223 The deduced cultural intervals were used as two extra dating points to validate the age
224 model build up with BACON software.

225

226 3.2. Paleomagnetic analyses

227 Forty-four paleomagnetic cylindrical samples were taken with a soft sediment
228 extraction device along the 232 cm sequence. Cores were cut to standard size (2.1 cm
229 height x 2.5 cm diameter) and 3 to 4 specimens were obtained from each cylinder.

230 Alternating field (AF) and thermal (TH) demagnetization procedures were carried out in
231 sister samples from the same cylinder. Prior to the demagnetization analyses, the
232 anisotropy of the magnetic susceptibility was measured in the KLY3 (AGICO Inc.) of
233 the University of Zaragoza to determine the petrofabric of the samples. The
234 demagnetization analyses were performed at the paleomagnetic laboratory of the
235 University of Burgos (Spain), using a 2G cryogenic magnetometer, ASC furnace and
236 AF incorporated to the 2G magnetometer.

237 The characteristic component was calculated using Remasoft (Chadima and Hrouda,
238 2006), which follows the Kirsvink (1980) approach to calculate the orientation of the
239 component and the maximum angular deviation error (MAD).

240 The Iberian reference paleomagnetic catalogue and the geomagnetic model predictions
241 were calculated for the SCS coordinates (42.4566 N, 0.03963 E) using the data in i)
242 Gómez-Paccard et al. (2006), ii) the three global geomagnetic field models,
243 ARCH3k.1, CALS3k.4 and CALS10k.1b (Donadini et al., 2006; Korhonen et al., 2008;
244 Korte and Constable, 2011; Korte et al., 2011) and iii) the SCHA.DIF.3k geomagnetic
245 model (Pavón-Carrasco et al., 2009). The expected dipole inclination for the SCS
246 coordinates is 61.3º.

247

248 3.3. Rock magnetic analyses

249 To obtain more information about the ferromagnetic carriers of the characteristic
250 remanent magnetization, 19 samples were selected to carry out standard rock magnetic
251 analyses in the Curie Balance (Advanced Variable Field Translation Balance -Petersen
252 Instruments-) at the University of Burgos. Acquisition of the isothermal remanent
253 magnetization (IRM) curves (up to 1 T), back field curves, hysteresis loops (from 0.75
254 T to -0.75 T) and thermomagnetic curves where the induced magnetization is measured

under an applied field of 27 mT from 40ºC to 700ºC (heating run) and back to 40ºC (cooling run), were performed in air in powder samples less than 400 mg.

4. Results

4.1. Stratigraphy of the waterlaid detrital record

The sedimentological characteristics of the studied sequence allow dividing the infilling of the detrital record from Seso Cave into five sedimentological units that correspond to two main sedimentary environments (Fig. 2).

Unit 1 (100 cm thick) is mainly composed of light grey and brownish laminated marls. Carbonate induration (calcrete) appears in the lower section. This unit corresponds to pond deposits (Jennings, 1985) and relates to the transport as suspended load of the autochthonous marls detached by piping processes and the deposition in stagnant water areas. This facies requires a low-energy environment, such as a small pond where suspended sediments have time to settle down prior to form a sediment layer (White, 2007). In the Seso Cave System occurrence of ponded water areas in the lower part of the main tilted linear passage is related to the obstruction by sediments of the narrow drainage conduit, which connects this gallery with lower ones.

Unit 2 is 80 cm thick, with a U-channel shape, and overlays the unit 1 incising it to the left of the profile where samples are taken. It is composed of ochre lutites with centimetric clasts displaying a fining-upward sequence and plant remnants. This unit represents stream sediments that erode the former unit. Channel incision requires the cleaning of the former obstruction favoring the drainage of the pond area and starting the runoff along the entire passage. That means a change of the base level in the vadose drainage of the cave. Neither paleomagnetic nor ^{14}C samples were taken in this unit.

Unit 3 (20 cm in thickness) is composed of ochre and grey lutites with bioturbation features and charcoal remnants. This unit corresponds to suspended load of autochthonous marls as well as allochthonous lutites deposited in shallow stagnant water areas with episodic subaerial exposure of sediments. Deposition was produced from small streams reaching ephemeral pond areas inside the cave.

Unit 4 (67 cm thick) is composed of lutites with orange colors, plant remnants, intercalated clasts (limestones, pottery remnants and bones) and features of root bioturbation. It represents the sedimentation, in marginal areas of an ephemeral stagnant water body, of allochthonous lutites transported by low-energy sheet floods. Subaerial exposure features increases in the upper part of the unit.

Units 3 and 4 are called mixed facies when paleomagnetic results are shown since they comprise alternations of stream and pond deposits. The proportion of stream facies increases towards the top of the units.

Unit 5 (53 cm thick) comprises ochre-orange sands with cross lamination, lutites and conglomerates. The top of this unit contains more sand with coarser grain size and cross-bedding lamination. Among the laminae, vesicular structures are observed, indicating a fast sedimentation rate (Bull, 1964). This unit corresponds to scour and fill channel deposits related to allochthonous inputs, being mostly made of the soil material observed outside the cave that was eroded by runoff processes and entered into the cave by small streams.

Summarizing, two main different sedimentary environments were found to occur throughout the Seso detrital sequence: i) stagnant water areas with settling of suspended sediments (unit 1) and ii) alluvial fan with sheet floods and channelized streams (increasingly present in units 2, 3, 4 and 5). Detrital deposited sediments are autochthonous (internal marls detached by piping processes) and allocthonous (external soil and weathered marls entered by surficial runoff). Stagnant water areas decrease along the sedimentary fill in the cave, disappearing in unit 5, which solely consists of stream deposits. Bioturbation features are also usual. Limestone clasts are, basically, breakdown deposits by failure. In addition, charcoal remnants are disseminated by streams along the whole profile.

It is remarkable the occurrence of two levels of human settlement in the cave located just below the beginning of the paleomagnetic profile and in the Unit 4 (on the left of Fig. 2). The lowermost one is characterized by soft pottery remnants, brownish in color, probably made from rudimentary fired raw clay, without temper. The pottery remnants of the upper level are bright red in color. Nevertheless, natural sedimentation was not noticeably modified by the human settlement.

315 4.2. Bayesian age model

316 The obtained age-depth model based on the seven AMS dates, displays a good degree of
317 agreement as the posteriors for accumulation rate and its variability are comparable to
318 their priors, as well as the internal correlation of the age series (memory) (Fig. 3). As
319 stated before, the time period recorded by the Seso sequence is between 2080 and 650
320 cal yr BP (Table 1) and despite sedimentation rate varies slightly (Table 2), the
321 accumulation process seems relatively fast and homogeneous for the lower part of the
322 sequence underneath the second human settlement, it is ~ 2.7 mm / yr in the first 140
323 cm (Units 1 and 3 and lower part of 4). Then for the upper part of the Unit 4 the
324 accumulation rate decreases to 0.8 mm / yr, (140- 190 cm) and increases again for Unit
325 5 to 1.2 mm / yr (190-232 cm) (Table 2).

326 It is important to notice that in the section where the paleomagnetic samples are taken,
327 the change from pond to the mixed facies starts at 100 cm from the bottom (~1710 cal
328 yr BP) and solely stream sediments are above 190 cm (~1000 cal yr BP). The mixed
329 facies occur between 100-190 cm.

330 The two pottery-enriched levels confirm the age-model: the lower one is dated as
331 Iberian Period (600 BC-200 AD) and the upper one is typified as cooking pottery of
332 *Terra Sigillata Africana* (Lamboglia 51/ Hayes 59), dated in the III AD century in
333 origin, and in the second half of the IV AD and V AD in the Ebro valley. Therefore the
334 settlement inside the cave occurred around century V AD most probably, since SCS is
335 situated in the Pyrenean realm, far from the Ebro valley (Bartolomé et al., 2013).

336

337 4.3. Paleomagnetic results

338 The values of the natural remanent magnetization (NRM) and bulk susceptibility (χ) are
339 related to the origin of the sediments (Fig. 4, Annex table I), with lower values at the
340 bottom of the profile (from paleomagnetic sample 3 to 23), which are mainly the pond
341 deposits (average of NRM: 1.04×10^{-3} Am^2/kg with standard deviation (s.d.) of $7.81 \times$
342 10^{-4}, and average of χ is 5.61×10^{-8} m^3/kg with s.d. of 2.14×10^{-8}) and increasing values
343 in the mixed and stream deposits, with average of NRM: 7.63×10^{-3} Am^2/kg and s.d. of
344 3.04×10^{-3}, and average of χ is 2.37×10^{-7} m^3/kg with s.d. of 5.51×10^{-8}.

All analyzed samples (except two) provide at least one reliable characteristic component calculated with 4 to 15 demagnetization steps, (Table 3, Figs. 5a, 5b). The characteristic component in the AF method is calculated between 10 to 90 (or 100) mT of the applied field, and the median destructive field (MDF) is for most of the samples below 20 mT. For the temperature demagnetization procedure, the component is calculated between 300º to 500º-580ºC with the exceptions in samples 1, 2, 3 and 16, where the unblocking temperature is 600º - 615ºC. The calculated characteristic component directs towards the origin except in some samples demagnetized with AF (i.e. samples 13, 16, 20, 21, 22, Figs. 5a, Table 3).

The alternating field (AF) demagnetizing method provides a more precise paleomagnetic component than the thermal (TH) demagnetizing method since the maximum angular deviation (MAD) errors in AF are below 10 for 95% of the samples respect to the 43% of the samples in the TH method (Table 3, Fig. 6a). However, some samples (10, 13, 15, 16, 17, 19, 27) are not completely demagnetized at 90 mT. Between 20% up to 40% of the remanent magnetization is not demagnetized at 90 mT (sample 13c, Fig. 5a, Table 3). The median destructing field in these samples is higher than 30 mT indicating the presence of a higher coercitive mineral; therefore the calculated paleomagnetic component may not be the characteristic one. For those samples, the thermal method carried out on the sister samples provides the characteristic component. The thermal demagnetization of these sister samples suggest the presence of a minimum quantity (the remanent magnetization left above 580ºC is less than 10%) of a high coercitive mineral with unblocking temperatures ≥ 600ºC (probably hematite). The erratic behavior of the demagnetization steps after 615ºC indicates that this high coercitive mineral does not carry a characteristic component (i.e., sample 13, but not shown in the decay of the NRM above 500ºC). The TH characteristic component directs towards the origin and is calculated up to 600ºC in samples where a minor quantity of hematite is present.

Comparing the declination and inclination values between sister samples (Fig. 6b, 6c) differences are below $|15^{\circ}|$ for 69% of the samples in declination values and 76% of the samples in inclination values. Especially good correspondence between sister samples is observed in the inclination diagram of the mixed and the stream facies. Higher differences between both methods can be related to i) the coercivity spectra does not

always correspond with the unblocking temperatures spectra for the calculated components of sister samples (see for example, sample 1 in Fig. 5b), ii) incomplete demagnetization using the AF method, i.e. 13c, 16d, Fig. 5a) iii) overlapping of components that cannot be resolved in the laboratory (curved demagnetization diagrams in AF), i.e. sample 24, 29, 32 Fig. 5a, 5b.

The standard deviation of declination and inclination values between sister samples (Fig. 6c) increases towards the upper part of the pond deposits (top of unit 2), where the sedimentation rate is higher than in the lower part of the pond deposits (Fig. 3). In the stream deposits, the inclination values are the closest between sister samples, with all values of inclination between sister samples being less than 15º apart. In addition to that, the largest standard deviation occur related to human settlements, better seen in the second human settlement, with values of standard deviation above 30º for inclination and above 40º for declination (sample 27). However, the bottom sample of the profile is also affected by the lower human settlement, with a standard deviation value in inclination above 40º.

4.4. Rock magnetic analyses

All the 18 analyzed samples in the Curie Balance indicate that the carrier of the remanence is a soft coercitive mineral with the acquisition of IRM curves that are saturated below 250 mT, and the values of the coercivity of the remanence obtained from the back field curves that have values between -20 and -40 mT, Fig 7. The Curie temperature obtained from the thermomagnetic curves are around 580ºC, indicating that magnetite is the ferromagnetic *s.l.* mineral present. In few samples there is a small contribution of a mineral with Néel temperature of 680ºC (sample 14a in Fig. 7) indicating the presence of hematite. However, all the back field experiments (even in the samples with some hematite) provide values of the coercivity of the remanence under -50 mT (Fig. 7, left), indicating the predominance of magnetite (soft coercitive magnetic mineral) in the samples.

The correction of the hysteresis loops for the paramagnetic content indicates that the paramagnetic fraction (most probably phyllosilicates) makes up more than 46% (except in two samples with 30%) in the first 120 cm of the profile (Units 1 and 3), where the

sediments have mainly an internal cave origin (reworked marls). In the upper part of the profile, the mixed and stream deposits, where the sediments have mainly an external origin from soils, there are less than 21% of paramagnetic minerals, indicating a predominance of the ferromagnetic fraction for this part of the profile (Table 4). These results confirm the higher value of NRM and bulk magnetic susceptibility of the stream sediments respect to the pond sediments (Fig. 4).

5. Discussion

The waterlaid detrital deposit of the Seso Cave System records unique environmental characteristics that can be reconstructed by the hydrological changes and variations recorded in the depositional environments. In addition, the detrital sedimentary sequence remains and can be observed thanks to the erosion of part of the profile due to the later water incision of the clastic deposit.

5.1. Paleoenvironmental reconstruction from the Seso Cave detrital record

The SCS detrital sequence covers from 2080 to 650 cal yr BP. The most important change takes place at about 140 cm corresponding, within age errors, to the end of the Roman Period (ca. 400-500 years AD). This transition represents a change in the sedimentation rate, with a strong decrease from 2.7 mm/yr to < 1.5 mm/yr This change in sedimentation rate occurs after the second human settlement, coeval with the beginning of the increasing amount of stream sediments. The most likely explanation for this sedimentation rate change is related to the water availability in the surrounding landscape of the cave. First, during the Roman Period, the increase in precipitation detected in the Iberian Peninsula (Martín-Puertas et al., 2010; Moreno et al., 2012 and references therein) would have allowed the continuous entrance of water into the SCS. Thus, inside the cave, pond deposits associated with the presence of water were formed. Later, after ca. 500 AD, an abrupt decrease in the sedimentation rate within the alluvial facies reflect the minor influence of the processes occurring at the interior of the cave and the dominance of the entrance of material from the exterior. This period (ca. 500 – 900 AD) correlates with the Dark Ages, a time characterized by low temperatures in other areas of Europe (Millet et al., 2009) and the Iberian Peninsula (Martín-Chivelet et

al., 2011) that would have reduced the water circulation inside the cave and favor the transition towards the stream facies. Later, the increase in the alluvial activity recorded in the upper part of the profile (Unit 5) with the coarser facies within the stream deposits, likely indicates an intensification of the arid environmental conditions, which degrade the vegetation cover and favor the surficial runoff. Sedimentation rate increases to 1.2 mm/yr in Unit 5, which occurs during the Medieval Climate Anomaly (900-1350 AD), an arid period recorded in several areas in the Iberian Peninsula (Martín-Puertas et al., 2010; Moreno et al., 2012). As a consequence of that climate aridification, soil erosion processes intensified as has also been observed at a regional scale in other detrital sequences (Peña et al., 2004; Sancho et al., 2008).

5.2. Paleomagnetic response of the Seso sediments recording secular variations

Considering the age of the paleomagnetic samples of the Seso Cave System we compare the declination and inclination results from both demagnetizing methods directly with i) the data of the reference paleomagnetic catalogue (Gómez-Paccard et al., 2006) calculated for the SCS coordinates (Annex table 2) and different geomagnetic models, ARCH3k.1, CALS3k.4 and CALS10k.1b (Donadini et al., 2006; Korhonen et al., 2008; Korte and Constable, 2011; Korte et al., 2011) and the SCHA.DIF.3k model for the last 3000 years of Pavón-Carrasco et al. (2009), Fig. 8.

It is noteworthy the lack of reference paleomagnetic data between 1545 and 925 cal yr BP (405-1025 yr AD) and therefore, any reliable paleomagnetic data from that period of time will be extremely useful for completing the Iberian paleomagnetic secular variation reference catalogue (ISVRC) and will help determining which geomagnetic model is closer to the actual data. Prior to that, the comparison of the SCS data with the reference catalogue (ISVRC) and the geomagnetic models will determine how reliable these clastic sediments are for recording paleomagnetic secular variations.

The samples that can be actually compared with the ISVRC and the models are summarized in Table 5 (Fig 8), and in general there is a poor overlapping of the new paleomagnetic data with either the ISVRC or the geomagnetic models (called reference curves from now on), only 6 samples overlap with both demagnetizing methods, the declination of the reference curves, and 9 samples overlap the inclination. However, it is

noteworthy the good quality of the stream deposits in recording the paleomagnetic inclination, since 6 samples (out of 9) reproduce the inclination of the reference curves with both demagnetizing methods. Due to this fact, we propose that the inclination data from the SCS youngest sediments should be considered in order to select the geomagnetic model closer to them. Therefore, the paleomagnetic results of the youngest sediments agree well with the CALS10k.1b geomagnetic model for the period where no archeomagnetic data are available.

5.3. Why overlapping of SCS with the reference curves is poor?

The poor overlapping of the actual new data with the reference curves can be due to different factors as we mentioned in the introduction, most of them related to depositional processes: flocculation, energy of the system and/or postdepositional factors: human occupation, sedimentary load, root bioturbation, or the statistical approach that produces a lack of accuracy. Looking at the paleomagnetic results we examine these factors in the sedimentary record of the SCS.

i) The higher proportion of paramagnetic material in the lower part of the section (Unit 1, pond facies from 0 to 100 cm), indicates a higher concentration of phyllosilicates (clays), see Table 4. These minerals can enhance flocculation. It has been tested that flocculation dominates in clay-rich sediments and thus plays an important role in remanence acquisition, that is, clay-rich sediments form larger flocs that reduce magnetic alignment efficiency. They are thus poor recorders of the geomagnetic field direction (Spassov and Valet, 2012 and references therein). To analyze the role of flocculation in Seso clayed sediments, the dispersion index was examined in the re-sedimented clays of Unit 1, giving a very high value, close to the maximum (1) (Bartolomé et al., 2013). This indicates that the redeposited marls are dispersive in the laboratory with an artificial dispersant added to the samples. However, flocculation in the natural marls can occur, and therefore, flocculation process cannot be discarded as an influence on the reduced accuracy of the remanence acquisition of the Seso karstic sediments (Marshall and Workman, 1977 in Bartolomé et al., 2013).

ii) The higher part of the profile (Units 3 and especially 4 and 5) is enriched in ferromagnetic minerals (lower clay content, lower flocculation effect) and the energy

related to the depositional environment is quite different from the lower part. The running water bringing in external soil (allogenic) dominates the transport of material into the cave from 140 cm to the top of the profile. Energy is higher and thus transported particles are coarser, particularly in Unit 5. Therefore, the record of the Earth magnetic field by these sediments might be affected by the higher energy of the sedimentation system (paleocurrents).

The energy of the sedimentary system can be seen by the petrofabric within the sediments with for example a preferred orientation due to a current flow. A method of studying petrofabrics is using the anisotropy of the magnetic susceptibility (AMS) (Graham, 1954). In the SCS karstic sediments, the petrofabric observed by the anisotropy of the magnetic susceptibility (Annex figure 1) suggests a typical unoriented sedimentary fabric, with the minimum axes (k_{min}) of the magnetic ellipsoid vertical, and the intermediate (k_{int}) and the maximum (k_{max}) axes of the magnetic fabric ellipsoid, distributed on the horizontal plane without any evident particular orientation. This information indicates that flow currents do not affect the sedimentation processes and hence, they do not induce an oriented petrofabric. Therefore we can discard the explanation of a high energetic system for the lack of overlapping of the SCS paleomagnetic data with the reference curves.

iii) The two periods of human occupation of the cave affect the orientation of the paleomagnetic direction due to compaction/removilization of the samples during those periods. This effect explains the high standard deviation between the values of sister samples (120-140 cm) and especially the anomalous magnetic declination of sample 27 (at 140 cm). In addition, only samples 1 and 4 (also possibly affected by the human occupation) show anomalous inclinations respect to the reference curves, and sample 1 has a high value of the standard deviation between the sister samples. Therefore, at least for the two periods of cave occupation, human activities in the cave may be responsible of sediment compaction and thus lack of coherence with the reference curve.

iv) The inclination shallowing that occurs sometimes in the geological record, especially in red beds, is discussed to be the result of the sedimentary load (Tan and Kodama, 2012 and references therein). Here in SCS, this load is negligible, however, the inclination in the lower part of the sequence (120 cm) is always lower than in the

reference curves (Fig. 8) suggesting that some inclination shallowing occurs, but this fact can be also related to flocculation and not to the sedimentary load.

v) Root bioturbation is especially important between 140-180 cm, (samples 27 to 35). From the 9 samples, six overlap with the inclination reference curve and CALS10k.1b model, and five samples for the declination values. Therefore, it seems that root bioturbation is not the main cause for the disturbance of the paleomagnetic signal.

vi) Finally, it has to be taken into account the number of samples. The reason of taken only one sample per level is to reproduce, with standard samples, the information obtained in a drill core and therefore, with the u-channel sampling technique. However, the appropriate number of samples is a requirement in order to have a statistical and meaningful paleomagnetic mean. For example, in paleopole studies 24 specimens are needed for a good quality paleopole calculation (i.e., N = 24), paleomagnetic studies about vertical axis rotations (N = 8) or paleomagnetic studies in archeological sites (N = 20) (Van der Voo, 1992; Butler, 1992; Gómez-Paccard et al., 2006). Therefore the high variation of declination and inclination values between sister samples may be due to the low statistical representativeness of the number of samples per level, that is, age (only one sample per level). However, due to the small size of the deposit, a parallel sampling profile is not available.

6. Conclusions

The waterlaid detrital cave sedimentary record in the Seso Cave System is composed of two different type deposits: a first autochthonous pond sediments and a second allochthonous stream deposits covering from 2080 to 650 cal yr BP. The main change in the sedimentary sequence took place at the end of the Roman Period when the general decrease in humidity produced a reduction of water inside the cave thus diminishing the importance of in-cave piping processes in the accumulation of the sediments. After ca. 900 AD, corresponding to the Medieval Climate Anomaly, an intensification of alluvial activity in the Pyrenees is coeval to an aridification trend in the regional landscape setting. The change of the sedimentation environment is also recorded by the magnetic content, with higher ferromagnetic content and higher magnetic susceptibility in the

stream deposits than in the pond deposits due to the entrance of soil material from the outside of the cave.

The paleomagnetic and rock magnetic analyses of the detrital sediments of the Seso cave indicate that a soft coercivity mineral is the main ferromagnetic carrier. The Curie temperature of 580ºC indicates magnetite as the main ferromagnetic mineral present in all samples. The presence in minor quantities of some high coercitive mineral with Néel temperature of 680ºC (hematite) observed in few samples (6) is revealed by the AF demagnetization, which is not completed at 90 mT. Hematite prevents the proper demagnetization AF procedure in some samples, therefore differences between sister samples are important. The lack of complete demagnetizations with the AF method points to prefer the thermal method, even though the AF characteristic component is more accurate than the TH characteristic component.

The comparison of the characteristic paleomagnetic component (declination and inclination) between sister samples demagnetized with TH and AF provides differences in declination higher than 15º in 13 sister samples (31%) and differences in inclination higher than 15º in 10 sister samples (24%).

The comparison of the paleomagnetic signal of the detrital sediments of the Seso cave with the reference catalogue of paleosecular variations of Iberia (ISVRC) and the geomagnetic models (reference curves) to test the reliability of the paleomagnetic record indicates:

i) The overlapping of the Seso paleomagnetic data with the reference curves is poor. The poor overlapping is difficult to explain looking at the depositional and postdepositional factors qualitatively and quantitatively analyzed. We suggest that the depositional processes such as energy of the sedimentation system and postdepositional process such as root bioturbation do not affect the accuracy of the paleomagnetic record of these sediments. However, flocculation and human settlements seem to affect the overlapping of the new data with the reference curves.

ii) Despite this poor overlapping with the reference curves, the paleomagnetic inclination is better recorded than the paleomagnetic

declination especially in the stream deposits, and both demagnetizing methods give similar results. Tentatively, the paleomagnetic inclination data recorded by the SCS stream deposits suggests that for inclination, the CALS10k.1b geomagnetic model reproduces better the actual data.

Acknowledgements

BOU acknowledges the JAEdoc programme of CSIC, partly financed by the European Social Fund. All authors thank the financial support of the Instituto de Estudios Altoaragoneses, of the projects CGL2009-10455/BTE (MICINN and FEDER), ORDESA (Autonomous Organism of National Parks), and the PaleoQ Group (Universidad de Zaragoza-Gobierno de Aragón). We are also indebted to Jaume Mas-Moiset and Xavier Fuertes from the Grup d'Espeleologia de Badalona (GEB) for the cartography of the cave system and field support. Dr. José Luis Peña-Monné and Dr. Fernando Pérez-Lambán are acknowledged for the classification and comments of pottery remnants. We are indebted to GEOMAGIA50, which is a database that comes with a web interface intended to give users easy access to archeomagnetic data (Donadini et al., 2006 and Korhonen et al., 2008).

References

Abrajevitch, A., Kodama, K. 2009. Biochemical vs. detrital mechanism of remanence acquisition in marine carbonates: A lesson from the K–T boundary interval. Earth and Planetary Science Letters 286, 269–277.

Bartolomé, M., Sancho, C., Moreno, A. Belmonte, Á, Muñoz, A., Osácar, M.C., 2011. La cueva de Seso (Boltaña, Huesca): aproximación geomorfológica y espeleogénesis holocena. Resúmenes XIII Reunión Nacional de Cuaternario Andorra, AEQUA 151-153.

Bartolomé, M., Sancho, C., Moreno, A. Belmonte, Á, Bastida, J., Calle, M, Mas, J., Fuertes, X. 2013. El papel del piping en la espeleogénesis del sistema endokárstico de Seso (Pirineo central, Huesca). Geogaceta 53 105-108.

Bilardello, D., Jezek, J., Gilder, S.A., 2013. Role of spherical particles on magnetic field recording in sediments: Experimental and numerical results. Physics of the Earth and Planetary Interiors 214, 1–13.

Blaauw M., Christen J.A., 2011. Flexible paleoclimate age–depth models using an autoregressive gamma process. Bayesian Analysis 6, 457–474.

Bosák, P., Pruner, P., Kadlec J., 2003. Magnetostratigraphy of Cave Sediments: Application and Limits. Studia Geophysica et Geodaetica 47, 301-330.

627 Bosch, R.F., White, W.B., 2007. Lithofacies and transport of clastic sediments in karstic
628 aquifers. In: Studies of cave sediments. Physical and Chemical records of paleoclimate.
629 Revised Edition. Editors: Ira D. Sasowsky and John Mylorie. Springer 329pp, 1-22.
630 Bull, W B., 1964. Alluvial fans and near surface subsidence in Western Fresno County,
631 California. U. S. Geol. Surv. Profess. Papers 437A, 1-71.
632 Butler, R.F., 1992. Paleomagnetism: Magnetic Domains to Geologic Terranes. Blackwell
633 Scientific Publications, 238pp.
634 Creer, K.M., Kopper, J.S., 1974. Paleomagnetic Dating of Cave Paintings in Tito Bustillo Cave,
635 Asturias, Spain. Science New Series 186, No. 4161, 348-350.
636 Creer, K.M., Kopper, J.S., 1976. Secular oscillations of geomagnetic-field recorded by
637 sediments deposited in caves in mediterranean region. Geophysical Journal of the Royal
638 Astronomical Society 45, 35-58. DOI: 10.1111/j.1365-246X.1976.tb00312.x.
639 Chadima, M., Hrouda, F., 2006. Remasoft 3.0 a user-friendly paleomagnetic data browser and
640 analyzer. Travaux Géophysiques XXVII, 20-21.
641 Channel, J.E.T., 2006. Late Brunhes polarity excursions (Mono Lake, Laschamp, Iceland Basin
642 and Pringle Falls) recorded at ODP Site 919 (Irminger Basin). Earth and Planetary
643 Science Letters 244, 378–393.
644 Chazan, M., Ron, H., Matmon, A., Porat, N., Goldberg, P., Yates, R., Avery, M., Sumner, A.,
645 Horwitz, L.K., 2008. Radiometric dating of the Earlier Stone Age sequence in Excavation
646 I at Wonderwerk Cave, South Africa: preliminary results Journal of Human Evolution 55,
647 1–11.
648 Donadini, F., Korhonen, K., Riisager, P., Pesonen, L., 2006. Database for Holocene
649 geomagnetic intensity information, EOS, Transactions, American Geophysical Union
650 87(14), 137.
651 Ford D.C., Williams P.W., 2007 - Karst Hydrology and Geomorphology. Wiley, 576 p.
652 Faust D., Zielhofer C., Baena R., Diaz del Olmo F., 2004. High-resolution fluvial record of late
653 Holocene geomorphic change in northern Tunisia: climatic or human impact? Quaternary
654 Science Reviews 23, 1757-1775.
655 Gómez-Paccard, M., Catanzariti, G., Ruiz-Martínez, V.C., McIntosh, G., Núñez, J.I., Osete,
656 M.L., Chauvin, A., Lanos, Ph., Tarling, D.H., Bernal-Cassola, D., Thiriot, J.,
657 Archaeological Working Group, 2006. A catalogue of Spanish archaeomagnetic data.
658 Geophysical Journal International 166, 1135-1143.
659 Gómez-Paccard, M., Larrasoaña, J.C., Sancho, C., Muñoz, A., McDonald, E., Rhodes, E.J.,
660 Osácar, M.C., Costa, E., Beamud, E., 2013. Environmental response of a fragile, semiarid
661 landscape (Bardenas Reales Natural Park, NE Spain) to Early Holocene climate
662 variability: A paleo- and environmental-magnetic approach. Catena 103, 30–43.
663 Hajna, N.Z., Mihevc, A., Pruner, P., Bosák, P., 2010. Palaeomagnetic research on karst
664 sediments in Slovenia. International Journal of Speleology 39 (2), 47-60.
665 Herries, A.I.R., Shaw, J. 2011. Palaeomagnetic analysis of the Sterkfontein palaeocave deposits:
666 Implications for the age of the hominid fossils and stone tool industries. Journal of
667 Human Evolution 60 (5), 523–539.
668 Katari, K., Tauxe, L., King, L., 2000. A reassessment of post-depositional remanent magnetism:
669 preliminary experiments with natural sediments. Earth and Planetary Science Letters 183,
670 147-160
671 Kirschvink, J.L., 1980. The least-squares line and plane and the analysis of paleomagnetic data.
672 Geophysical Journal of the Royal astronomical Society 62, 669-718.

673 Korhonen, K., Donadini, F., Riisager, P., Pesonen, L., 2008. GEOMAGIA50: an archeointensity
674 database with PHP and MySQL, Geochemistry, Geophysics, Geosystems 9,
675 doi:10.1029/2007GC001,893.
676 Korte, M., Donadini, F., Holme, R., 2011. Reconstructing the Holocene geomagnetic field.
677 Earth and Planetary Science Letters 312, 497–505.
678 Korte, M. and Constable, C., 2011. Improving geomagnetic field reconstructions for 0-3 ka.
679 Physics of the Earth and Planetary Interiors 188, 247-259. doi:
680 10.1016/j.pepi.2011.06.017.
681 Jennings, J.N., 1985. Karst Geomorphology. Basil Blackwell, 293 p. Oxford.
682 López-Martín F., Cabrera-Millet M., Cuadrat J. M., 2007. Atlas Climático de Aragón. Dirección
683 General de Calidad Ambiental y Cambio Climático. Departamento de Medio Ambiente.
684 Gobierno de Aragón. 222 p., Zaragoza.
685 Marshall, A.F., Workman, J.P., 1977. In: Dispersive clays, related piping and erosion in
686 geothecnical projects. Editors: J.L. Sherard, R.S.Decker. American Society for Testing
687 and Materials 623, 274-286.
688 Mas, J., Fuertes, X. 2007. Cueva del caserío de Seso (Huesca). CIJA de Teruel 2, 30-32
689 Martín-Chivelet, J., Muñoz-García, M.B., Edwards, R.L., Turrero, M.J., Ortega, A.I., 2011.
690 Land surface temperature changes in Northern Iberia since 4000 yr BP, based on **d**13C of
691 speleothems. Global and Planetary Change 77, 1-12.
692 Martín-Puertas, C., Jiménez-Espejo, F. Martínez-Ruiz, F., Nieto-Moreno, V., Rodrigo, M.,
693 Mata, M.P., Valero-Garcés, B. L., 2010. Late Holocene climate variability in the
694 southwestern Mediterranean region: an integrated marine and terrestrial geochemical
695 approach. Climate of the Past 6, 807–816.
696 Millet, L., Arnaud, F., Heiri, O., Magny, M., Verneaux, V., Desmet, M., 2009. Late-Holocene
697 summer temperature reconstruction from chironomid assemblages of Lake Anterne,
698 northern French Alps. The Holocene 19, 317-328.
699 Mitra R., Tauxe., L., 2009. Full vector model for magnetization in sediments. Earth and
700 Planetary Science Letters 286, 535–545.
701 Moreno, A., Pérez, J., Frigola, V., Nieto, M., González-Sampériz, P., Morellón, M., Martín-
702 Puertas, C., Corella, J.P., Belmonte, A., Cacho, I., Canals, M., Jiménez-Espejo, F.,
703 Martínez Ruiz, F., Vegas, T., Valero-Garcés, B., 2012. The Medieval Climate Anomaly
704 in the Iberian Peninsula reconstructed from marine and lake records. Quaternary Science
705 Reviews 43, 16-32.
706 Musgrave. R.J., Webb, J.A., 2003. Palaeomagnetic analysis of sediments in the Buchan Caves,
707 southeastern Australia, provides a pre-Late Pleistocene date for landscape evolution. In:
708 Studies of cave sediments. Physical and Chemical records of paleoclimate. Revised
709 Edition. Editors: Ira D. Sasowsky and John Mylorie. Springer 329pp, 47-70.
710 Noel, M., 1986. The palaeomagnetic and magnetic fabric of sediment from Peak Cavern,
711 Derbyshire. Geophysical Journal of the Royal Astronomical Society 84, 445-454.
712 Noel, M., St. Pierre, S., 1984. The palaeomagnetic and magnetic fabric from Gronligrotta and
713 Jordbrugrotta, Norway. Geophysical Journal of the Royal Astronomical Society 78, 231-
714 239.
715 Noel, M., Shaw R.P., Ford, T.D., 1984. A palaeomagnetic reversal in Early Quaternary
716 sediments in Mason Hill, Matlock, Derbyshire, Mercian Geolol 9, 235-242.
717 Peña, J.L., Julián, A., Chueca, J., Echeverría, M.T., Ángeles, G., 2004. Etapas de evolución
718 holocena en el valle del río Huerva: Geomorfología y Geoarqueología. In: Geografía
719 Física de Aragón: aspectos generales y temáticos. Editors: Peña, J.L., Longares, L.A.,
720 Sánchez, M. Universidad de Zaragoza-Institución Fernando el Católico 289–302.

Pavón-Carrasco, F. J., Osete, M. L., Torta J. M., Gaya-Piqué, L. R., 2009. A regional archeomagnetic model for Europe for the last 3000 years, SCHA.DIF.3K: Applications to archeomagnetic dating, Geochemistry Geophysiscs Geosystems 10, Q03013, doi:10.1029/2008GC002244.

R Development Core Team, 2011. R: R: A Language and Environment for Statistical Computing. Vienna, Austria: the R Foundation for Statistical Computing. ISBN: 3-900051-07-0. http://www.R-project.org/.

Reimer, P.J., Bard, E., Bayliss, A., Beck, J.W., Blackwell, P.G., Ramsey, C.B., Buck, C.E., Cheng, H., Edwards, R.L., Friedrich, M., 2013. IntCal13 and Marine13 radiocarbon age calibration curves 0–50,000 years cal BP. Radiocarbon 55, 1869–1887.

Sancho, C., Peña, J.L., Muñoz, A., Benito, G., McDonald, E., Rhodes E.J., Longares, L.A., 2008. Holocene alluvial morphopedosedimentary record and environmental changes in the Bardenas Reales Natural Park (NE Spain). Catena 73, 225-238.

Sasowsky, I.D., White, W.B., Schmidt, V.A., 1995. Determination of stream-incision rate in the Appalachian plateaus by using cave-sediment magnetostratigraphy. Geology 23, 415-418.

Séguret, M., 1972. Étude tectonique des nappes de séries décollées de la partie centrale du versant sud des Pyrénées. Caractère synsédimentaire, rôle de la compression et de la gravité. Thèse Doct. Publ. USTELA. Série Géol. Montpellier. 155 pp.

Soto, R., Casas, A.M., 2001. Geometría y cinemática de las estructuras norte-sur de la cuenca de Aínsa. Revista de la Sociedad Geológica de España 14 (3-4), 199-211.

Spassov, S., Valet, J.P., 2012. Detrital magnetizations from redeposition experiments of different natural sediments. Earth and Planetary Science Letters 351-352, 147–157.

Stock, G.M., Granger, D.E., Sasowsky, I.D., Anderson, R.S., Robert C., Finkel, R.C., 2005. Comparison of U–Th, paleomagnetism, and cosmogenic burial methods for dating caves: Implications for landscape evolution studies. Earth and Planetary Science Letters, 236, 388–403.

Tan, X., Kodama, K.P., 2002. Magnetic anisotropy and paleomagnetic inclination shallowing in red beds: Evidence from the Mississippian Mauch Chunk Formation, Pennsylvania. Journal of Geophysical Research 107, doi: 10.1029/2001JB001636.

Turner G.M., Lyons, R.G., 1986. A palaeomagnetic secular variation record from c. 120000 yr-old New Zealand cave sediments, Geophysical Journal of the Royal Astronomical Society 87, 1181-1192.

Van der Voo, R., 1992. Paleomagnetism of the Atlantic, Tethys and Iapetus ocean. Cambridge University Press. 411pp.

White, W.B., 1988. Geomorphology and Hydrology of karst terrains. Oxford University Press, 464 pp. New York.

White, W.B., 2007. Cave sediments and paleoclimate.Journal of Cave and Karst Studies 69 (1), 76–93.

Zielhofer C., Faust D., Linstadter J., 2008. Late Pleistocene and Holocene alluvial archives in the Southwestern Mediterranean: Changes in fluvial dynamics and past human response. Quaternary International 181 (1), 39-54.

TABLE 1: AMS radiocarbon dates with the corresponding depth (cm) and the calibrated ages using the INTCAL13 calibration curve implemented in BACON. Columns represent the identification of the sample in the AMS laboratory of Seattle. Cm of the paleomagnetic section (from top and from bottom). The type of the material dated. The age of the sample with error and the final calibration with BACON in R.

Lab ID	cm from bottom	Type of material	AMS ^{14}C dates (yr BP)	errors	Calibrated ages (yr BP)	2-sigma values
D-AMS 001341	230	charcoal	707	25	668.5	18.5
D-AMS 001344	192	charcoal	1063	26	966	37
D-AMS 001343	168	charcoal	1697	23	1588.5	40.5
D-AMS 001342	138	charcoal	1772	23	1675.5	64.5
D-AMS 001345	125	charcoal	1785	77	1711.5	166.5
D-AMS 001346	52	charcoal	1714	26	1598	41
D-AMS 001347	4	charcoal	2175	36	2207	106

773
774

775 TABLE 2: Mean sedimentation rate for different sections of the Seso sequence with the
776 modelled ages.

Depth range (cm from bottom)	Age range (cal yr BP)	Mean sedimentation rate (mm/yr)	Period
232-190	650-1013	1.2	Medieval Climate A.
190-140	1013-1575	0.8	Dark Ages
140-0	1575-2080.5	2.7	Roman Period

777

778

779
780

781 TABLE 3: Calculated characteristic component, cm from bottom is the position of the sample,
782 sample number, DEC: declination, INC: inclination, MAD: maximum angular deviation, mT:
783 militesla, steps, and NRM left at 90 (100 mT)/ to 0,0: calculated component directs to the origin
784 of the orthogonal diagram. AF: alternating field demagnetization, TH: thermal demagnetization.

cm from bottom	SAMPLE	DEC AF	INC AF	MAD AF	mT	steps	NRM left /to 0,0	SAMPLE	DEC TH	INC TH	MAD TH	ºC	steps
232	SE44b	-23.6	48.9	1.9	10-100	12		SE44c	-29.7	50	4.7	360-500	5
225	SE43b	-5.3	51.8	2.5	14-100	10		SE43a	-3.2	47.5	16.7	430-530	4
220	SE42c	10.1	56.2	1.7	12-100	11		SE42b	1.2	57.9	3.7	400-500	4
213	SE41c	-18.5	54.8	3	12-100	11		SE41b	-1	55.5	5.1	360-500	5
206.5	SE40c	-9.5	47.1	1.5	12-100	11		SE40b	-17.3	57.4	13.9	430-530	4
200	SE39c	-6.3	54.9	3.3	18-100	8		SE39b	-19.1	49.8	8.5	400-550	6
195	SE38b	-38.3	66.7	3.1	20-100	7		SE38c	-4.7	77.4	4.4	330-500	6
190	SE37c	8.4	52.2	1.4	14-100	10		SE37b	3.5	56.5	6.1	360-500	6
185	SE36c	-3.5	52.8	1.3	14-90	9		SE36b	15.3	55.8	4.1	330-500	7
180	SE35c	-13.5	55.9	2.5	18-100	8		SE35b	0	53.5	3.5	300-500	6
175	SE34b	-4.9	49.9	1.4	14-100	10		SE34c	-2.1	45.7	2.8	400-500	4
170	SE33c	0	56.2	1.5	20-100	7		SE33b	-19	56.5	3.4	300-500	7
165	SE32c	24.4	45.2	2.6	10-100	12		SE32b	1.5	50.5	5.1	400-530	6
160	SE31c	-16.3	46.6	0.9	8-100	13		SE31b	-19.4	50.2	3.8	300-530	8
155	SE30c	-9.7	57.5	0.9	14-90	9		SE30b	-8.9	55.5	5.5	460-550	4
150	SE29c	29.8	43.4	7.9	40-90	4		SE29b	-13.4	50.2	2.9	330-580	9
145	SE28c	-8.3	65.8	1.6	10-100	12		SE28b	6	55.9	2.8	400-550	5
140	SE27c	125.5	48.5	1.5	16-100	9	20%	SE27b	135.8	51.3	19.6	430-580	7
135	SE26c	7.7	61.7	7.4	30-90	5		SE26b	-16.6	18.8	9.1	300-550	10
130	SE25c	0.5	60.2	6.9	30-90	5		SE25b	4.9	41.8	5.8	300-530	8
125	SE24c	-27.8	58.3	1.4	14-90	9		SE24b	-24.1	9.3	20.2	330-500	6
120	SE23c	-9.2	48.3	2.6	18-90	6		SE23b	-12.1	53.4	4.5	250-500	8
115	SE22c	8.1	51.5	1.8	10-50	9	/NO	SE22b	-2.5	54.8	6.7	360-530	6
110	SE21c	-15.4	53	2.5	10-50	9	/NO	SE21b	-12.3	58.3	5	300-530	8

105	SE20c	11.7	56.1	1.2	10-30	7	/NO	SE20b	15.1	52.7	9.3	400-530	5
100	SE19c	-28.6	48.4	10.2	18-90	7	10%	SE19b	6.4	58.5	4.4	330-580	9
93	SE18c	-9.8	45.3	6	30-90	4		SE18b	9.5	46.5	7.8	360-500	5
86.5	SE17c	-2.5	11.5	4.2	30-90	5	30%	SE17b	-28.1	52.3	13	430-580	6
80	SE16d	-18	16.5	1.6	70-90	2	30%	SE16b	-7.4	59.8	25.5	360-600	9
75	SE15d	-8.7	22.8	6.1	30-90	5	30%	SE15a	14.4	47.4	11.8	360-580	8
70	SE14c	-25.4	55.2	4.1	8-90	11	10%	SE14b	-4.9	59.3	13.7	250-500	8
65	SE13c	-14.3	17.6	6.6	40-90	4	40%	SE13b	-3	43.1	18	400-500	4
60	SE12c	-21.6	45.7	9.3	8-90	11		SE12b	-21	18.7	18.7	300-500	7
55	SE11b	-0.8	50.8	2.4	8-90	11		SE11c	7	60.3	16.7	330-460	6
50	SE10c	-2.4	45.6	8.8	4-90	13	30%	SE10b	1.8	32.4	15.8	200-530	10
45	SE9a	-5.1	57.4	5.6	18-90	7		SE9b	-2.8	65.4	13.1	360-430	4
41	SE8c	-11.6	44.3	11.8	16-90	8		SE8b	1.6	47.7	16.7	200-530	11
35	SE7c	-12.8	48.1	8.8	10-90	11	20%	SE7b	-14	54.5	13.6	300-500	10
30	SE6c	10.8	24.3	13.5	20-40	3	NO	SE6b	4.6	46.2	16.2	200-530	10
25	SE5b	9	40	11	30-70	5	20%	SE5a	4.9	45	25.4	300-530	11
20	SE4a	-	-	-	-	-		SE4b	-29	-43.4	16.3	330-500	7
10	SE3c	-	-	-	-	-		SE3b	-12.2	59.7	7.6	200-600	13
5	SE2d	-5.7	51.1	5.6	21-90	9	10%	SE2b	-16.3	54	4.3	250-600	12
0	SE1b	-12.5	-9.3	2.2	10-90	11		SE1a	-30.3	55.8	8.5	500-615	6

785

786

Table 4: Paramagnetic and ferromagnetic content after correcting the hysteresis loops of the selected samples.

Sample name	%para.	%ferro.
SE-44b	3.09	96.91
SE-43a	10.45	89.55
SE-40a	13.18	86.82
SE-38d	16.24	83.76
SE-36c	17.60	82.40
SE-34d	19.93	80.07
SE-32a	15.72	84.28
SE-30d	15.25	84.75
SE-28a	8.61	91.39
SE-26d	20.79	79.21
SE-23d	46.53	53.47
SE-20a	46.75	53.25
SE-18a	30.82	69.18
SE-14a	30.31	69.69
SE-11d	76.16	23.84
SE-10a	74.79	25.21
SE-8a	43.11	56.89
SE-6d	60.63	39.37
SE-2d	71.59	28.41

Table 5: SCS paleomagnetic data that overlaps with the reference curve or models envelopes separated in facies and demagnetization procedure. AF: alternating field demagnetization, TH: thermal demagnetization. Samples with asterisk indicate differences in declination (inclination) with the sister samples higher than 20º. See Figure 8 for graphic representation.

DECLINATION

	Both (AF and TH)	AF	TH
Stream deposits	42, 30	37, 28, 25	36, 29*, 26*
Pond deposits	10, 9, 5	18, 17, 11, 2	22, 16, 14, 13, 8, 6
Mixed	23	33	32

INCLINATION

	Both (AF and TH)	AF	TH
Stream deposits	44, 43, 41, 40, 39	42	37, 29, 28, 27
Pond deposits	14	9	16*, 11, 7, 3
Mixed	33, 30, 22	35, 21, 20	36, 23, 19

802
803 FIGURE CAPTIONS

804 Fig. 1. Location of the SCS. 1a, b) Orthophoto with the location of the two caves and the
805 seasonal spring. 1b) Profile and topography of the cave with the location of the karstic
806 sediments profile. 1c) Picture of the NE corner of the cave.

807 Fig. 2. Picture of the sedimentary profile with location of paleomagnetic (Pm) (white dots) and
808 charcoal (^{14}C) (black bar) samples. The two enriched-pottery levels (human settlements) are also
809 marked with white arrows. On the right, the sedimentological profile with the sedimentary units
810 and environments.

811 Fig. 3. Age model. At the bottom, the calibrated radiocarbon dates using the INTCAL13
812 calibration curve implemented in BACON (Y axis) with the corresponding depth (cm in the X
813 axis). In black bars, the human occupation levels of the cave. At the top, the three graphs
814 represent the robustness of the age model, which automatically tune the Monte Carlo Markov
815 Chain simulation (Blaauw and Christen, 2011). See text for more details.

816 Fig. 4. Values of the natural remanent magnetization (NRM) and bulk susceptibility (χ)
817 normalized by mass of all standard-sized samples. Actual values are in Annex table 1. Notice
818 the lower values of the pond deposits respect to the stream deposits. Vertical black bars
819 represent the human occupation levels next to the sedimentary environments.

820 Fig. 5. a and b) Paleomagnetic demagnetization diagrams. Orthogonal projection and decay of
821 the remanence for selected samples. In the orthogonal diagrams black (white) circles are the
822 projection of the declination (inclination) at every step.

823 Fig. 6.a) Values of paleomagnetic declination and inclination for the alternating field
824 demagnetization (red squares) and thermal demagnetization (green triangles) procedures. Black
825 vertical bars on the righ, the human occupation levels of the cave. b) Differences between the
826 two demagnetizing methods (AF and TH) in declination and inclination. In dark grey,
827 differences lower than 15º and light yellow for differences between 15º and 20º for declination
828 and inclination. c) On the right, the standard deviation of the values in declination (blue) and
829 inclination (yellow) of sister samples.

830 Fig. 7. Rock magnetism analyses. a) Isothermal remanent magentization (blue) and back field
831 (red) of the remanent magnetization. b) Variation of the induced magnetization during heating
832 (red) and cooling (blue). c) Enlargement of the heating curve of b).

833 Fig. 8. Comparison of the actual values of declination and inclination (AF and TH methods) in
834 the SCS with the ISVRC (for the SCS coordinates) and the geomagnetic models in age.

Numbers in black are erased samples far from the reference curves and with large differences with the sister sample. Numbers in colours indicate samples within the reference curves, i) blue, both demagnetizing methods lie in the reference curves, ii) red, only the AF demagnetized sample lie in the reference curve, iii) green, only TH demagnetized sample lie in the reference curve.

Annex table 1: NRM and χ data.

Annex table 2: Catalogue from Gómez-Paccard et al., 2006 in Seso coordinates.

Annex figure 1: Anisotropy of magnetic susceptibility. Squares: maximum magnetic axes, triangles: intermediate axes and circles: minimum axes of the magnetic ellipsoid.

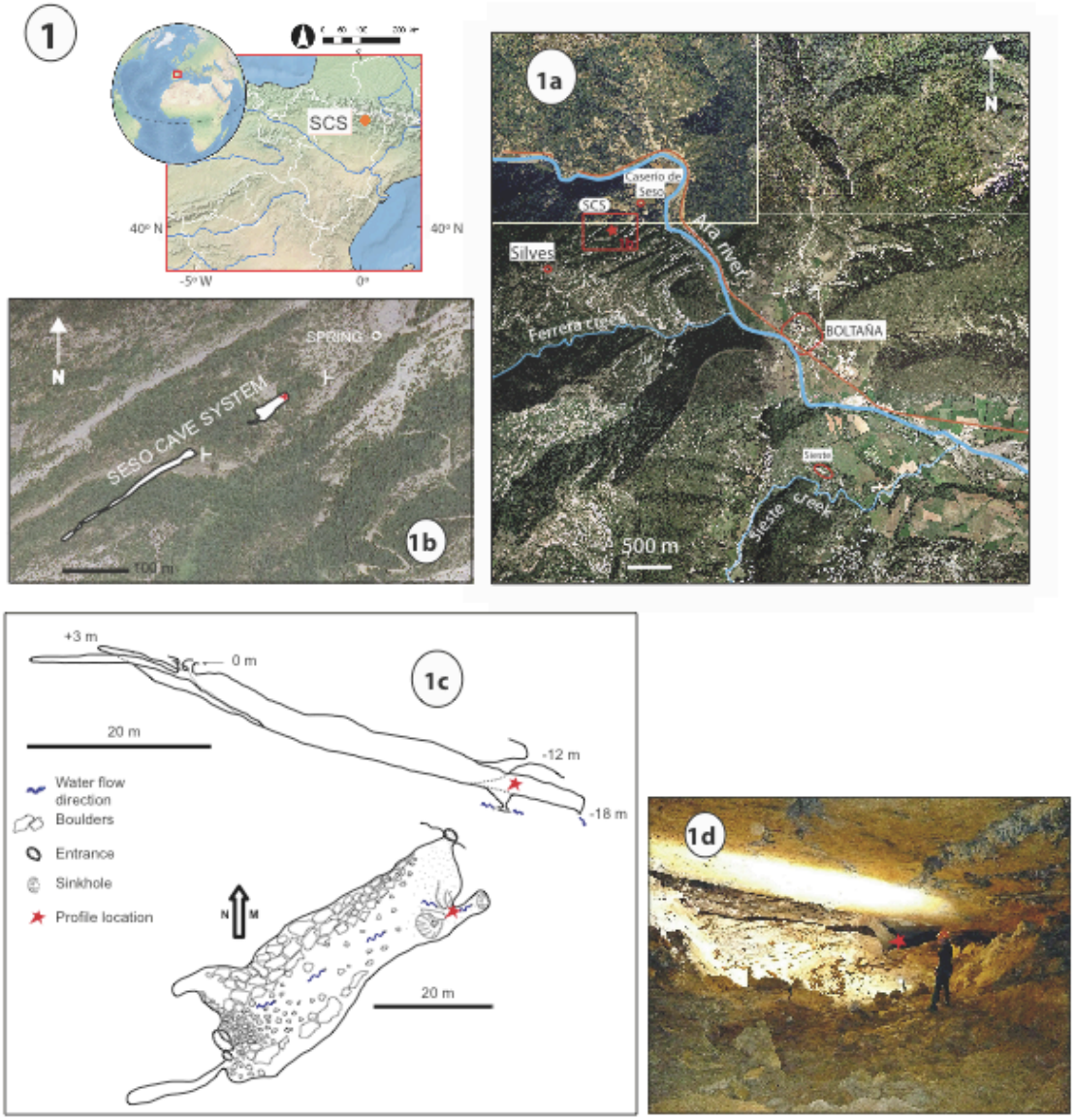
1
SCS
40º N
40º N
-5º W
0º
1a
N
Caserío de Seso
SCS
Silves
Ara river
Ferrera creek
BOLTAÑA
Sieste creek
500 m
N
SPRING
SESO CAVE SYSTEM
1b
100 m
+3 m
0 m
1c
20 m
-12 m
-18 m
Water flow direction
Boulders
Entrance
Sinkhole
Profile location
N
20 m
1d

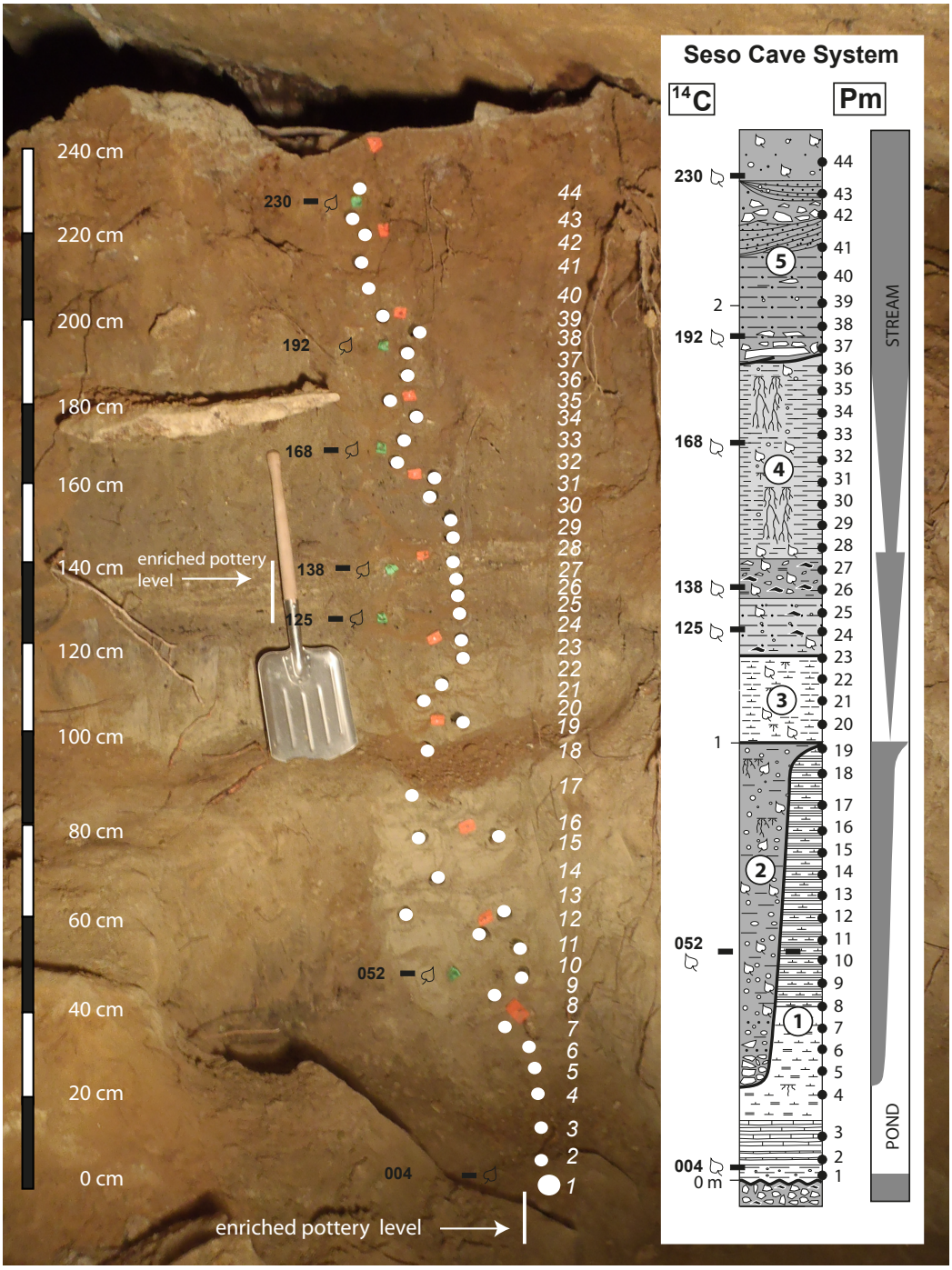
240 cm
220 cm
200 cm
180 cm
160 cm
140 cm
120 cm
100 cm
80 cm
60 cm
40 cm
20 cm
0 cm
enriched pottery level
230
192
168
138
125
052
004
enriched pottery level
Seso Cave System
14C
Pm
STREAM
POND
0 m
LEGEND
Units
Conglomerates
Sands
Lutites
Marls
Calcretes
Vesicular structures
Plant remnants
Charcoal
Bioturbation
Parallel lamination
Ceramics
Sandy silt matrix
Clayey silt matrix

Fig. 2

849

850

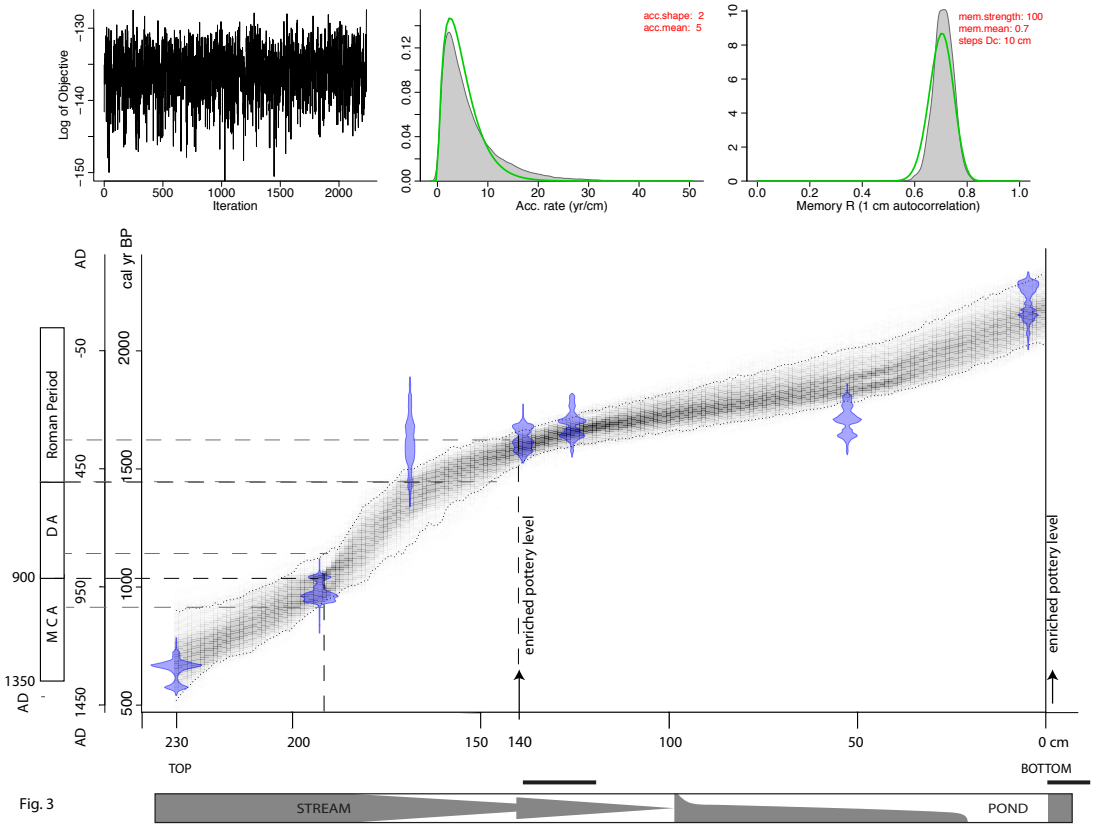
Log of Objective
Iteration
acc.shape: 2
acc.mean: 5
Acc. rate (yr/cm)
mem.strength: 100
mem.mean: 0.7
steps Dc: 10 cm
Memory R (1 cm autocorrelation)
cal yr BP
AD
Roman Period
D A
M C A
AD
enriched pottery level
enriched pottery level
TOP
BOTTOM
STREAM
POND

Fig. 3

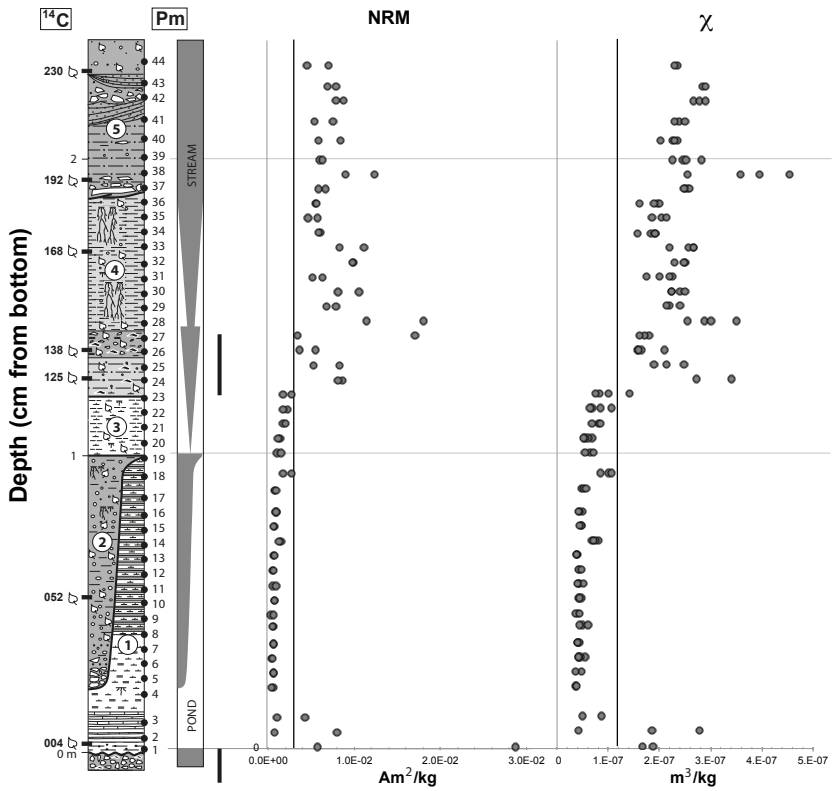
14C
Pm
NRM
χ
Depth (cm from bottom)
230
192
168
138
125
052
004
0 m
STREAM
POND
0.0E+00
1.0E-02
2.0E-02
3.0E-02
Am2/kg
0
1.E-07
2.E-07
3.E-07
4.E-07
5.E-07
m3/kg

Fig. 4

Fig. 5 a

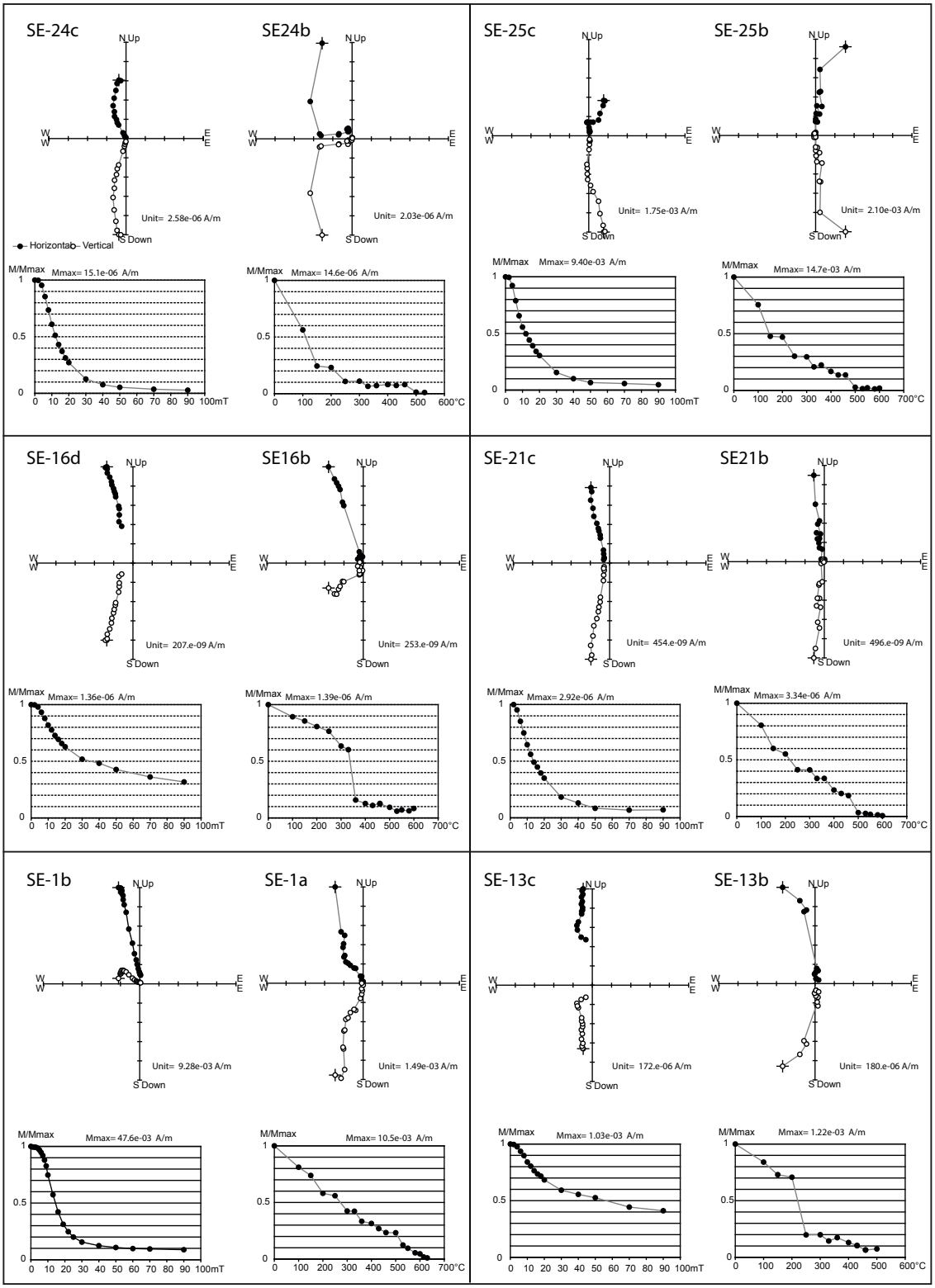
SE-24c
SE24b
SE-25c
SE-25b
SE-16d
SE16b
SE-21c
SE21b
SE-1b
SE-1a
SE-13c
SE-13b
N Up
S Down
W
E
Horizontal
Vertical
Unit= 2.58e-06 A/m
Unit= 2.03e-06 A/m
Unit= 1.75e-03 A/m
Unit= 2.10e-03 A/m
Unit= 207.e-09 A/m
Unit= 253.e-09 A/m
Unit= 454.e-09 A/m
Unit= 496.e-09 A/m
Unit= 9.28e-03 A/m
Unit= 1.49e-03 A/m
Unit= 172.e-06 A/m
Unit= 180.e-06 A/m
M/Mmax
Mmax= 15.1e-06 A/m
Mmax= 14.6e-06 A/m
Mmax= 9.40e-03 A/m
Mmax= 14.7e-03 A/m
Mmax= 1.36e-06 A/m
Mmax= 1.39e-06 A/m
Mmax= 2.92e-06 A/m
Mmax= 3.34e-06 A/m
Mmax= 47.6e-03 A/m
Mmax= 10.5e-03 A/m
Mmax= 1.03e-03 A/m
Mmax= 1.22e-03 A/m
0 10 20 30 40 50 60 70 80 90 100mT
0 100 200 300 400 500 600°C
0 100 200 300 400 500 600 700°C

859

Fig 5b

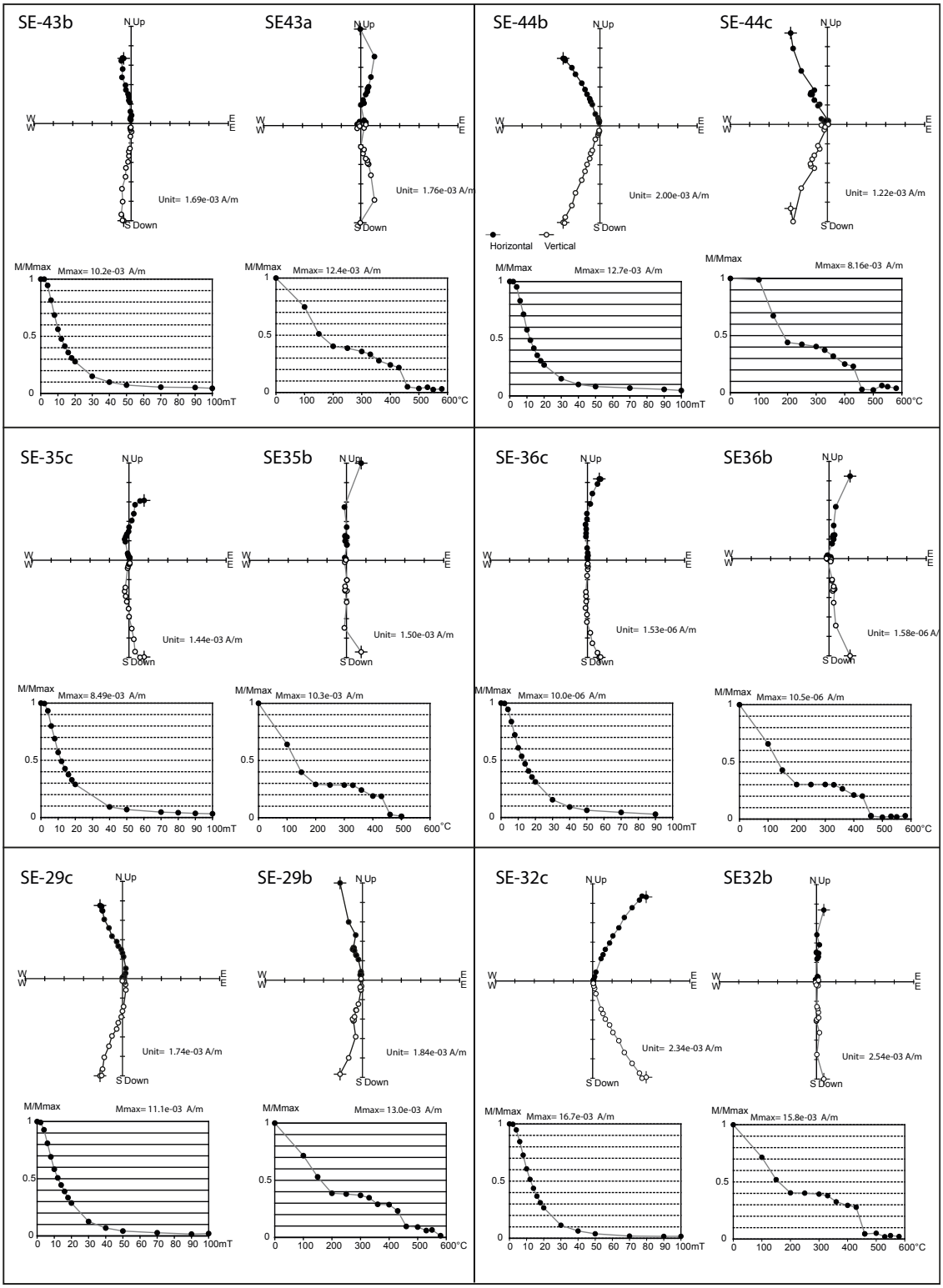
SE-43b
N Up
W
E
S Down
Unit= 1.69e-03 A/m
M/Mmax
Mmax= 10.2e-03 A/m
0 10 20 30 40 50 60 70 80 90 100mT
SE43a
N Up
Unit= 1.76e-03 A/m
S Down
M/Mmax
Mmax= 12.4e-03 A/m
0 100 200 300 400 500 600°C
SE-44b
N Up
Unit= 2.00e-03 A/m
S Down
Horizontal
Vertical
M/Mmax
Mmax= 12.7e-03 A/m
0 10 20 30 40 50 60 70 80 90 100mT
SE-44c
N Up
Unit= 1.22e-03 A/m
S Down
M/Mmax
Mmax= 8.16e-03 A/m
0 100 200 300 400 500 600°C
SE-35c
N Up
Unit= 1.44e-03 A/m
S Down
M/Mmax
Mmax= 8.49e-03 A/m
0 10 20 30 40 50 60 70 80 90 100mT
SE35b
N Up
Unit= 1.50e-03 A/m
S Down
M/Mmax
Mmax= 10.3e-03 A/m
0 100 200 300 400 500 600°C
SE-36c
N Up
Unit= 1.53e-06 A/m
S Down
M/Mmax
Mmax= 10.0e-06 A/m
0 10 20 30 40 50 60 70 80 90 100mT
SE36b
N Up
Unit= 1.58e-06 A/
S Down
M/Mmax
Mmax= 10.5e-06 A/m
0 100 200 300 400 500 600°C
SE-29c
N Up
Unit= 1.74e-03 A/m
S Down
M/Mmax
Mmax= 11.1e-03 A/m
0 10 20 30 40 50 60 70 80 90 100mT
SE-29b
N Up
Unit= 1.84e-03 A/m
S Down
M/Mmax
Mmax= 13.0e-03 A/m
0 100 200 300 400 500 600°C
SE-32c
N Up
Unit= 2.34e-03 A/m
S Down
M/Mmax
Mmax= 16.7e-03 A/m
0 10 20 30 40 50 60 70 80 90 100mT
SE32b
N Up
Unit= 2.54e-03 A/m
S Down
M/Mmax
Mmax= 15.8e-03 A/m
0 100 200 300 400 500 600°C

860

Fig. 6

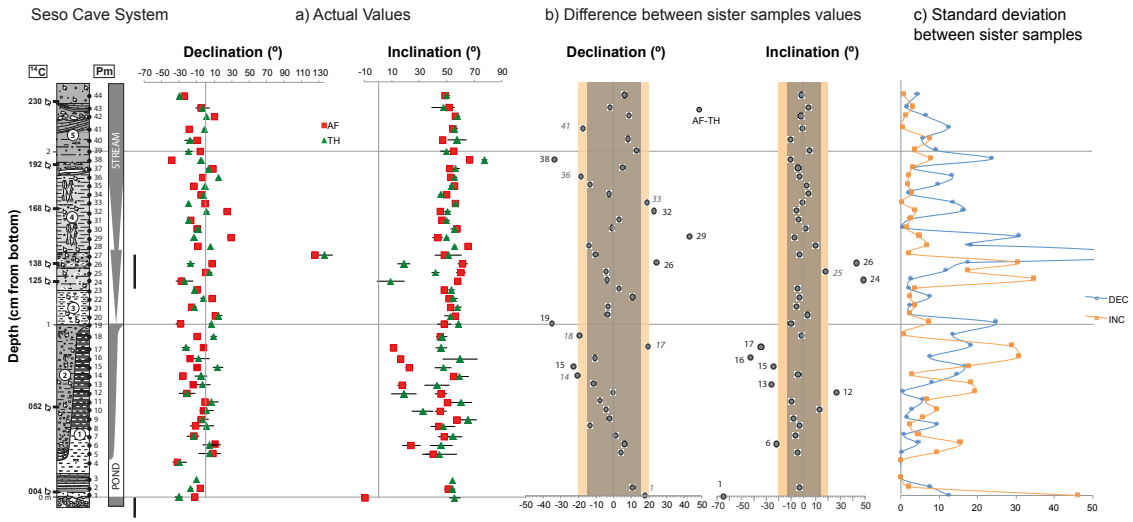
Seso Cave System
a) Actual Values
b) Difference between sister samples values
c) Standard deviation between sister samples
Declination (º)
Inclination (º)
Declination (º)
Inclination (º)
Depth (cm from bottom)
STREAM
POND
AF
TH
AF-TH
DEC
INC

861

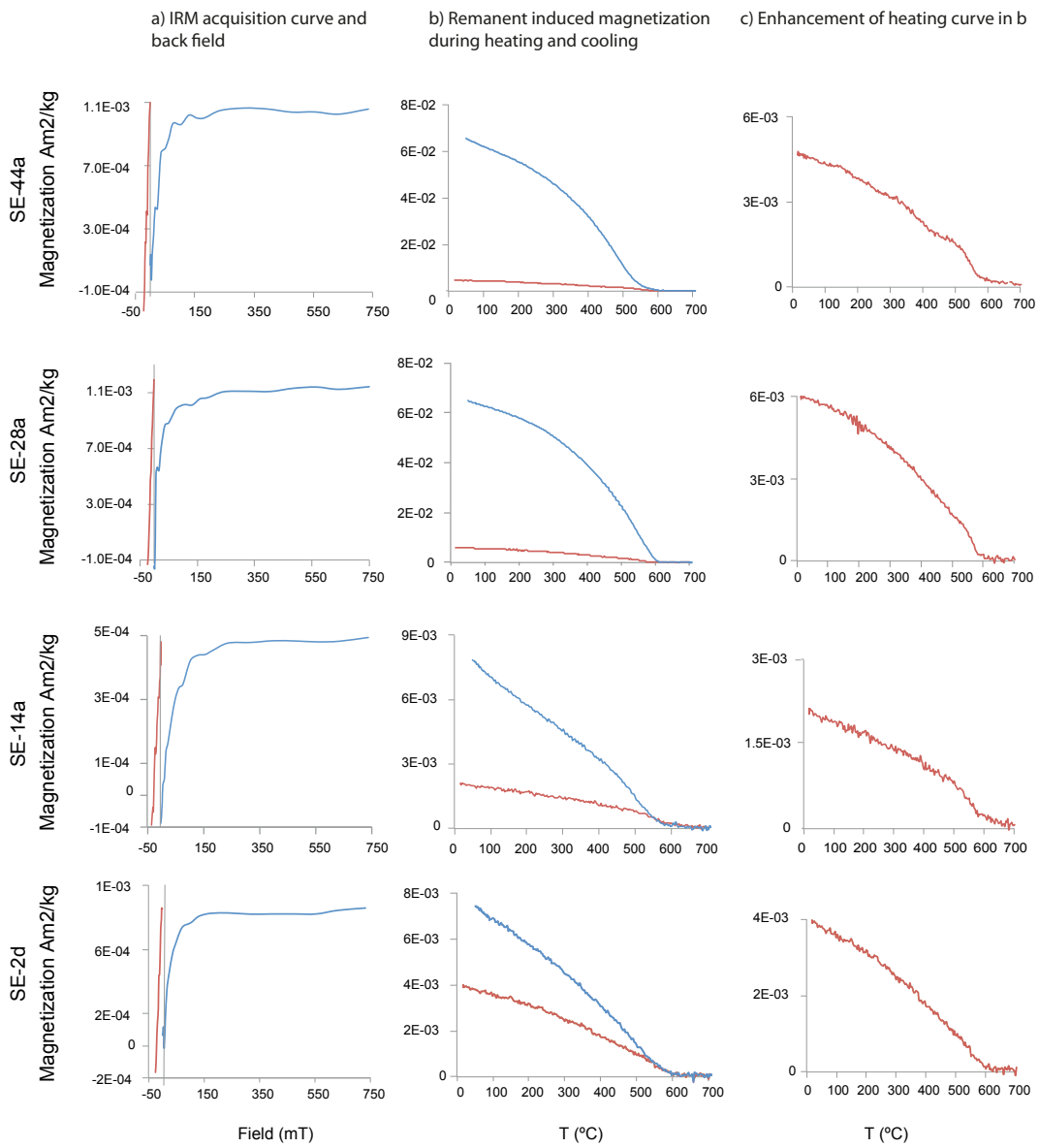
a) IRM acquisition curve and back field
b) Remanent induced magnetization during heating and cooling
c) Enhancement of heating curve in b
SE-44a
SE-28a
SE-14a
SE-2d
Magnetization Am2/kg
Field (mT)
T (°C)
T (°C)

Fig. 8

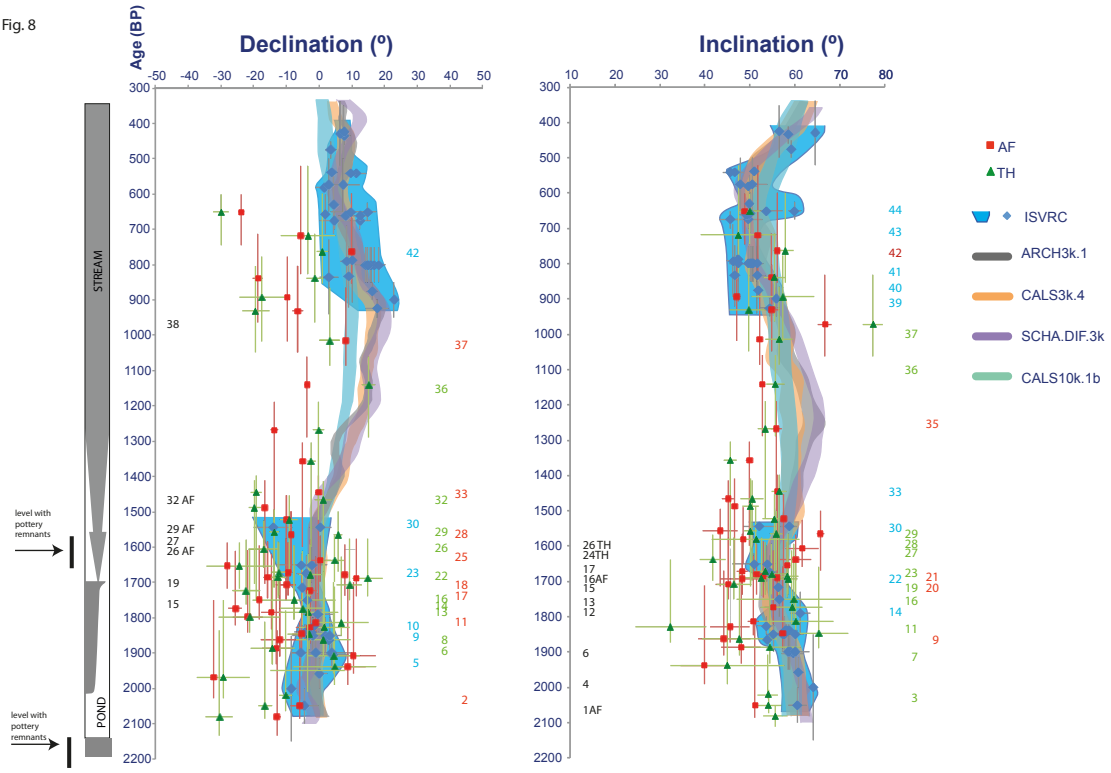
Age (BP)
Declination (º)
Inclination (º)
STREAM
POND
level with pottery remnants
level with pottery remnants
AF
TH
ISVRC
ARCH3k.1
CALS3k.4
SCHA.DIF.3k
CALS10k.1b

863